Research Article

# A New Method in Improving the Accuracy of Fetal Brain Health Diagnosis Based on Analysis of Constrictors Feature in Ultrasound Images

S. Surani<sup>a</sup> and M. Emadi<sup>b,\*</sup>

a Master Student, Department of Bioelectric Engineering, Ragheb Isfahani, Institute of Higher Education, Isfahan, Iran b Department of Electrical Engineering, Mo.C., Islamic Azad University, Isfahan, Iran

 $* Corresponding \ Author \ Email: \\ \underline{mehranemadi49@iau.ac.ir}$ 

DOI:10.71498/ijbbe.2025.1195960

**ABSTRACT** 

Received: Jan. 09, 2025, Revised: Apr. 23, 2025, Accepted: May 10, 2025, Available Online: Jul. 14, 2025

Fetal growth is a critical stage in prenatal care that requires the timely identification of abnormalities in ultrasound images to protect the health of the fetus and mother. Ultrasound-based imaging has played an essential role in diagnosing fetal malformations and abnormalities. Despite significant advances in ultrasound technology, detecting abnormalities in prenatal images still poses considerable challenges. These challenges often arise from time constraints and the need for substantial expertise from medical professionals. The aim is to classify several K classes of random forest support vector machine (SVM) and use this for evaluation. The aim is to perform a multi-class classification of 3 health stages, including healthy, suspicious, and diseased brain. Methods based on machine learning are among the methods that help experts. In this research, a machine learning method based on image scattering features is presented for the classification of fetal brain ultrasound images. In the proposed method, after integration, which is based on the maximum integration rule in scattered features, and discrete wavelet and cosine transform, a method based on the mutual information is presented for feature selection. The selected features have been used to diagnose the health status of the fetus with the help of the nearest neighbor. The evaluation criteria of accuracy, recall rate, accuracy and F criterion have been used for evaluation. The support vector machine classifier has shown its superiority in comparison with other classifiers with 98% accuracy, 97% accuracy, 99% recall rate, and F-criterion more than 98%. The comparison of the results obtained in the diagnosis of the health status of the fetus compared to other methods shows the superiority of the proposed method.

#### KEYWORDS

Improvement, Diagnosis, Fetal Brain Health, Ultrasound Images, Scattered Transform, Discrete Wavelet Transform.

## I. INTRODUCTION

Pregnancy is a significant and joyous phase in a woman's life that necessitates careful attention to maternal health. As a comprehensive assessment of fetal health prior to birth, it is essential for effective monitoring and outcomes. The fetus is dependent on the

mother in terms of the exchange of oxygen and carbon dioxide in the placenta, and this, in turn, depends on the sufficient concentration of gases in the mother's blood, the amount of blood in the uterus, the placenta's exchanges, and gas transfer to the fetus. A defect in any of the above factors can lead to a lack of oxygen in the fetal tissues (hypoxia), which, despite the presence of compensatory mechanisms, may cause an abnormal increase in the level of acid in the blood (acidosis) [2]. To monitor the growth and development of the fetus, several laboratory tests are suggested every trimester. One of these tests is ultrasound imaging, which is usually used in clinical evaluation to check the health status of the fetus in the womb [3]. The main goal is to monitor or diagnose the possible disease of different parts of the fetus, especially the brain, which can prevent the possible death of the fetus. If there is a system that can predict the future state of the fetus according to the current state, it can prevent problems such as miscarriage or serious injuries [4]. Determining fetal health is a difficult process that depends on various input factors. Depending on the input symptoms, the health status of the fetus is diagnosed. Sometimes it is difficult to determine the diagnosis of diseases, and there may always be differences of opinion between specialist doctors. As a result, the diagnosis of diseases is often performed in uncertain conditions and can sometimes cause undesirable errors. Therefore, the vague nature of diseases and incomplete patient data can lead to uncertain decision-making. One of the effective approaches to solve such a problem is the use of methods based on machine learning and deep learning in the diagnostic system [5]. Machine learning is widely used in studies related to fetal health diagnosis. Traditional machine learning techniques require manual feature extraction before classification. However, for automated analysis of neuron imaging data, manual feature extraction cannot accurately detect fetal brain health [6]. Approaches based on user-defined features in classical machine learning have limitations. Improved performance can be achieved by learning specific features to achieve the desired result. In the traditional machine learning based

method, pattern recognition processes are used. In this category of methods, after applying preprocessing on the image, numerous features, including textural, spectral, geometric and statistical features are extracted from the target image. These features are reduced in another step with the help of methods based on principal component analysis PCA, independent component analysis LDA. At this stage, feature selection methods can be used to select the most effective features [7,8]. Methods such as SFFS hierarchical forward feature selection or methods based on information theory, such as maximum correlation and minimum correlation mRMR can be used. Finally, the selected features are classified with the help of classifications such as support vector machine SVM, k-nearest neighbor KNN, and random forest RF. In this category of methods, a learning criterion or clustering methods are used to check the presence of lesions in the images. In the traditional methods of machine learning and pattern recognition, Euclidean, Mahalolunbis, or Shahr Block learning criteria are also used [9]. In the pre-processing, noise removal is done, and it is associated with image quality improvement processes. Feature extraction includes the use of different descriptors to find unique features from each image [10]. The most common descriptors used for feature extraction are transform domain methods such as discrete Fourier transform. discrete wavelet transform, discrete cosine transform, space domain-based methods such as internal and statistical features, and image histogram. building Methods based on information, such as local binary patterns, extracting effective features from images, are an essential step in diagnosing fetal brain health in ultrasound. The extracted features are used to create a one-to-one mapping between the target images. Extracting unique features is very important in creating accurate one-to-one mapping [11]. In the last decade, there have been many tendencies towards extraction with scattered representation. Because in this representation, there are almost only a small number of non-zero coefficients, or they have been scattered after applying transformations on the image. This trend seems

to be due to the potential to reconstruct the signal or image from a smaller number of measurements than conventional methods to reconstruct an entire signal. The features extracted in scatter transformations are more unique. One of the significant scatter transforms is the use of wavelet transform. The purpose of wavelet transform is a desirable strategy to establish an optimal balance between time accuracy and frequency accuracy. At higher frequencies, the wavelet transforms gains temporal information at the cost of losing frequency information. While frequencies, it gains frequency information at the expense of temporal information loss. This favorable approach to information exchange is useful for digital signal processing and music applications. Machine learning algorithms can presented for segmentation classification of normal and abnormal fetal brain ultrasound images. Through the studies, it was found that although there have been many studies and researches to determine the health of the fetal brain in ultrasound images, there is still a long way to go before reaching a favorable answer in the classification and diagnosis of these images. According to the studies conducted in the review of the research literature and the background of the research, it is clear that the methods based on image scattering transformations such as wavelet transformation and its group can provide effective and suitable features for this work. Based on the presented content, the innovations of this research can be stated as follows:

Using scattering transform based on the wavelet transform to detect fetal brain health stage in ultrasound images.

Using feature selection methods to identify informative data in ultrasound images.

The goal of this study is to implement a classification of multiple K classes using random forest and support vector machine (SVM) methodologies for evaluation. This classification will focus on three health stages: healthy, suspicious, and diseased brain.

# II. LITERATUREANDRE LATED WORKS

#### A. Research Background

In [12], a complex neural network (ECNN) model is used, which combines basic models to classify fetal plates using an open-access database containing 12,400 images with six fetal plates. Previous studies on this database included advanced CNN methods, and the pretrained Densenet-169 model provided an accuracy of 93.6%, which is presented as a deep learning model named FetSAM. The [13], proposed model is an advanced deep learning model, which aims to revolutionize fetal head ultrasound segmentation and thereby increase the accuracy of prenatal diagnosis. In [14], a crossover randomized control three-way method (trial registration: ChiCTR2100048233) reported evaluating the effectiveness of a deep learning system, the Prenatal Ultrasound Diagnosis Artificial Intelligence Behavior System (PAICS), in helping to detect fetal intracranial malformations. In [15], a U-Net fetal head measurement tool is presented, that uses a hybrid dice and binary cross-entropy loss to calculate the similarity between actual and predicted regions. Reference [16] has proposed to use ultrasound images in a deep learning model to automate fetal organ classification. The proposed model has been trained and tested on a dataset of fetal ultrasound images, including two datasets from different regions, and they have been recorded with different machines to ensure the effective detection of fetal organs. In [17], ultrasound images were analyzed using a Dense Net model. The accuracy of the trained model in correctly identifying cystic hygroma cases evaluated. This evaluation was conducted by calculating sensitivity, specificity, and the area under the receiver operating characteristic (ROC) curve. In [18], to investigate the application of Deep Learning Neural Network (DLNN) algorithms to identify and optimize the ultrasound image to analyze the impact and value in the diagnosis of fetal central nervous system (CNSM) malformation. It was in the diagnosis of ultrasound images (before birth) by

designing and implementing a new framework called Defending Against Child Death (DACD) [19]. The existing method is a semi-automatic method in which the Convolution Neural Network (CNN) algorithm is used to classify ultrasound images. In [20], the maturity of current deep learning classification techniques was evaluated for their application in a real maternal and fetal clinical setting. In [21], has proposed two main methods based on deep convolution neural networks for automatic detection of six standard fetal brain screens. One is a deep convolutional neural network (CNN) and the other is domain transfer learning based on CNN. The suggested methods in diagnosing fetal brain health in ultrasound images have low accuracy. The quality of the classification affects the diagnostic accuracy of the systems because many features, such as shape, aspect ratio, and border smoothness, are related to the contour of the region involved in brain pain. Furthermore, an automatic and realtime classification system may help radiologists identify disease in the fetal brain and provide a signal in case of human error.

#### **B.** Scattered Representation Analysis

Scattered representation is a way to reduce natural or artificial observations to their basic components. These signals often have scattered representation in a domain with regard to the place or time in which they usually appear. For tasks such as compression or parsing, it is often more efficient and meaningful to transform a signal into another domain or to find its scattered representation among a collection of basic signals, called atoms, that make up a dictionary. Analytical dictionaries have precise definitions that make them convenient in some situations, but are generally difficult and inefficient. For greater consistency, scattered coding methods were introduced to allow atoms from a mix of different cultures to be selected and added to represent signals [22]. Following this paradigm shift, Olshausen and field were among the first to propose a way to train a dictionary on examples associated with the desired signal [23]. Other algorithms, such as the K-SVD dictionary learning algorithm, are widely used today [24].

#### C. Discrete Cosine Transform (DCT)

Discrete cosine transform (DCT) represents a signal as a superposition of cosine waveforms with different frequencies. This transform is similar to the Discrete Fourier Transform (DFT) but only deals with real domain numbers. More importantly, DCT is more efficient in representing limited signals. This is because the Fourier Transform implicitly assumes a periodic expansion of a signal, which creates a discontinuity at the boundaries for most signals. Conversely, DCT assumes an anti-symmetric expansion to the signal. This problem leads to creating more sine waves to represent the signal with DFT than with DCT. The two-dimensional DCT transform of a signal x with dimensions M and N is:

$$A(p,q) = \alpha_p \alpha_q \sum_{m=0}^{M-1} \sum_{n=0}^{N-1} x(m,n) \cos \frac{(2m+1)\pi p}{2M} * \cos \frac{(2n+1)\pi p}{2N} 0 \le p \le M-1$$

$$\cos \frac{(2n+1)\pi p}{2N} 0 \le q \le N-1$$

$$\frac{1}{\sqrt{M}} p = 0$$

$$\alpha_p = \{ \frac{1}{\sqrt{M}} p = 0 \\ \sqrt{2/M} \ 1 \le p \le M - 1$$
 (1)

$$\alpha_q = \{ \frac{1}{\sqrt{N}} q = 0$$

$$\sqrt{2/N} \ 1 \le q \le N - 1$$

The DCT inverse transform is used to reconstruct the signal:

$$x(m,n) = \sum_{p=0}^{M-1} \sum_{q=0}^{N-1} \alpha_p \alpha_q A(p,q) \cos \frac{(2m+1)\pi p}{2M}$$

$$* \cos \frac{(2n+1)\pi q}{2N} 0 \le p \le M-1$$

$$0 \le q \le N-1$$
(2)

In this reconstruction of those basic functions

 $\alpha_p \alpha_q A(p,q) \cos \frac{(2m+1)\pi p}{2M} \cos \frac{(2n+1)\pi q}{2N}$  form a dictionary and by the coefficients if A(p,q). are integers, the number of atoms is equal to the size of the signal  $(M \times N)$  and the dictionary is orthogonal. Figure 1, shows an orthogonal

dictionary. Because of its simplicity, the orthogonal dictionary has often been used in the past, but relaxing this restriction allows sparse representations of signals.

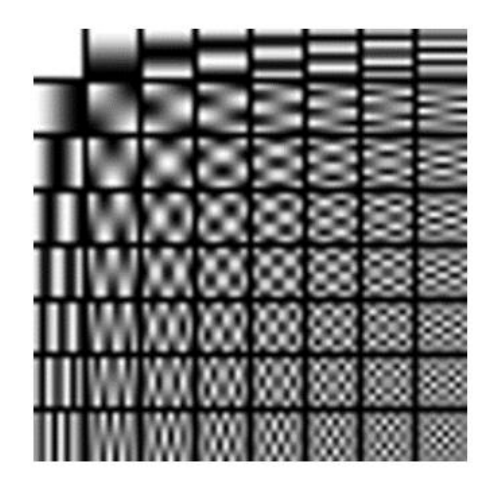


Fig. 1. Orthogonal DCT dictionary with 64 atoms of size 8x8.

This is achieved by allowing non-integer values for p and q, thereby increasing the number of atoms beyond the size of the signal. An example of such an overcomplete dictionary is shown in Figure 2.

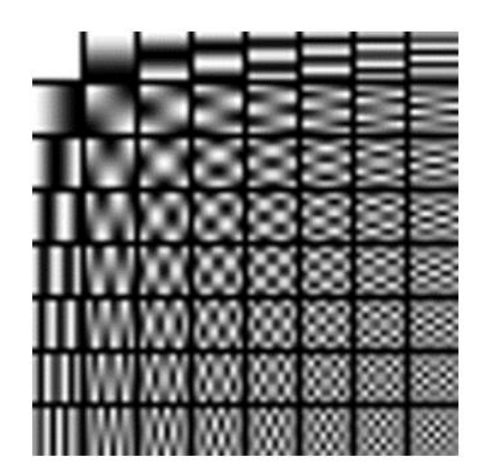


Fig. 2. Overcomplete DCT dictionary with 256 atoms of 8x8 dimensions.

## D. Discrete Cosine Transform

Wavelet transform can be calculated by equation (3):

$$C(a,b) = \frac{1}{\sqrt{a}} \int_{-\infty}^{\infty} f(x) \psi^*(\frac{x-b}{a}) dx \tag{3}$$

The  $\psi$  basis wavelet is designed to be reversible and computationally efficient. In practice, the translation and scaling parameters are as  $a = a_0^m$ ,  $b = nb_0a_0^m$  as  $m \cdot n \in \mathbb{Z}$ ,  $a_0 > 1 \cdot b_0 \cdot \text{Disc} > 0$  are discrete in this case. The wavelet transform (DWT) becomes:

$$C(m,n) = \frac{1}{\sqrt{a_0^m}} \int_{-\infty}^{\infty} f(x) \psi^* \left( \frac{x - nb_0 a_0^m}{a_0^m} \right) dx \qquad (4)$$

The signal *f* can be reconstructed by summing the weighted wavelets:

$$f = \sum_{m,n} c_{m,n} \tag{5}$$

The following values are usually used: a0 = 2, b0 = 1. There are  $\psi$  options where the set of wavelets  $\psi m, n$  form a canonical basis, in which case the wavelets are critically in. Each scale is sampled to accurately capture the newly introduced details. The scale of the simplest such wavelet is the scattering wavelet (Figure 3). Various other wavelets have been designed by Stromberg [25], Meyer [26], Daubeshiz [27] and others.

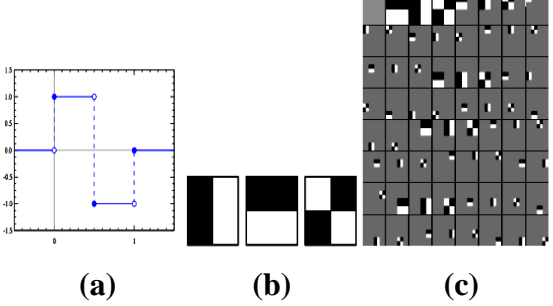


Fig. 3. a: 1D Haar wavelet, b: three configurations of Haar wavelet in 2D. Black color is negative and white is positive, c: Haar orthogonal dictionary consisting of wavelet expansion and translation.

In higher dimensions, the DWT is just a separable one-dimensional transform. So, for an image, first the columns and then the rows are individually transformed in the same way as any 1D signal. This makes DWT translation and rotation sensitive in higher dimensions. To overcome this issue, the Stationary Wavelet Transform (SWT) was introduced by Beylkin [28], which ignores orthogonality in favor of over-completeness. This is achieved removing subsampling and summing all translations of wavelet atoms.

# III. Methodology

The main goal of this research is to diagnose the health of the fetal brain with the help of image scattering features. In this regard, fetal brain ultrasound images should be pre-processed in a standard way. The block diagram of the proposed method is shown in Figure 4. In the following, different parts of the proposed method will be examined.

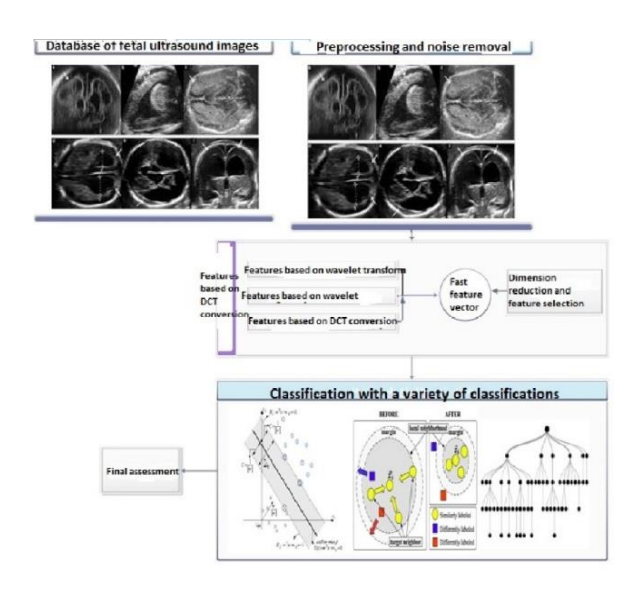


Fig. 4. The block diagram of the proposed method.

#### A. Preprocessing

In this paper, a fast algorithm for grayscale images is proposed as an adaptive two-way filter, which is otherwise computationally expensive and complex. This can be extended filtering color using channel-wise processing. Bidirectional filtering is used as an edge preservation tool in image enhancement applications. Along with a low-pass spatial core (which helps with smooth scattering), it uses a core to prevent smoothing near the edges. As a result, the filter can smooth homogeneous areas and preserve sharp edges at the same time. Gaussian spatial and domain cores were shown to improve the upscaling capacity of the twoway filter by adjusting the width and center of the curved range at each pixel. A two-way filter is shown as equations 6 and 7:

$$g(t) = \eta(i)^{-1} \sum_{j \in \Omega} w(j) \Phi_{i}(f(i-j) - \theta(i)) f(i-j) \quad (6)$$

$$\eta(i) = \sum_{j \in \Omega} w(j) \phi_{i}(f(i-j) - \theta(i)) \quad (7)$$

$$\eta(i) = \sum_{j \in \Omega} w(j)\phi_i(f(i-j) - \theta(i))$$
 (7)

In this article, spatial and locative cores will be used in the form of equations 8 and 9:

$$w(j) = \exp\left[-\frac{\|j\|^2}{2\rho^2}\right] \tag{8}$$

$$\Phi_{i}(t) = \exp\left[-\frac{t^{2}}{2\sigma^{2}}\right] \tag{9}$$

In the above equation,  $\sigma(i)$ ,  $\rho$  are effective width and bandwidth Gaussian window. In this way,  $\Omega = [-3\rho, 3\rho]^2$  unlike the classic bilateral filter, which uses a fixed-amplitude kernel in each pixel, the width  $\sigma(i)$  is allowed to change in each pixel in (8) and (9). In addition, the center of f(i) can be different from f(i) used in the classical two-way filter. Figure 5 shows the improved image with the help of the bilateral filter.







Fig. 5. An example of the improved image in the filtering method.

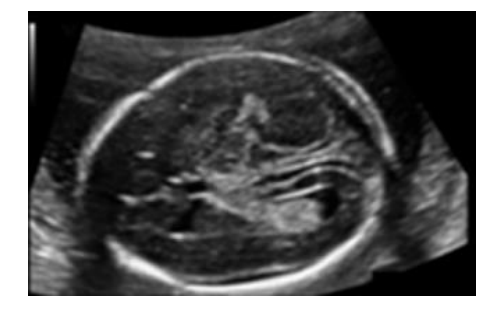
#### **B.** Scattered Transformers

# **B.I.** Scattered Representation Analysis

The curve transformation, which is a combination of the previous two transformations, allows us to analyze the image with different block sizes. The work process is that first, the image is decomposed into a set of wavelet bands, and the analysis of each band is performed by the Regretted transformation. The size of the blocks can be changed in each

level. In fact, it is a two-dimensional transformation that cannot be separated into one-dimensional transformations parallel to the coordinate axes. Curve transformation is presented for optimal representation of two-dimensional discontinuities. In this research, 2 levels of curve transformation are used. Figure 6a shows the feature map of level 1, and Figure 6b shows the feature map of level 2 of the curve transformation. The feature vector obtained from these two levels will be included in the feature vector of each pixel.

#### Contourlet coefficients Level 1





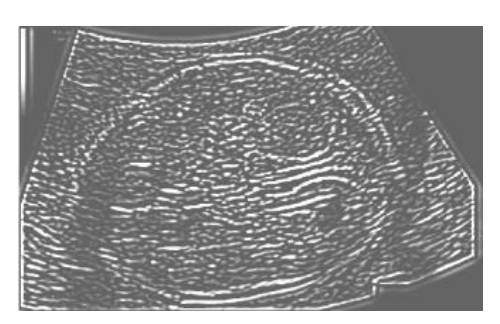


Fig. 6. Sub-bands created from curve transformation in a: level one, b: level two.

#### B.II. DCT implementation

The DCT algorithm is a compression and scattering algorithm to extract image scattering features. Due to the slowness of the previous calculation methods in the reviewed articles, at this stage, by applying this algorithm, we

increase the processing speed to a great extent. By compressing the image, it scatters the image and reduces the processing load to the program imposes. Figure 7 shows the process of applying the discrete cosine transformation function. Also, Figures 3- 6 show the scattered images by the DCT algorithm.

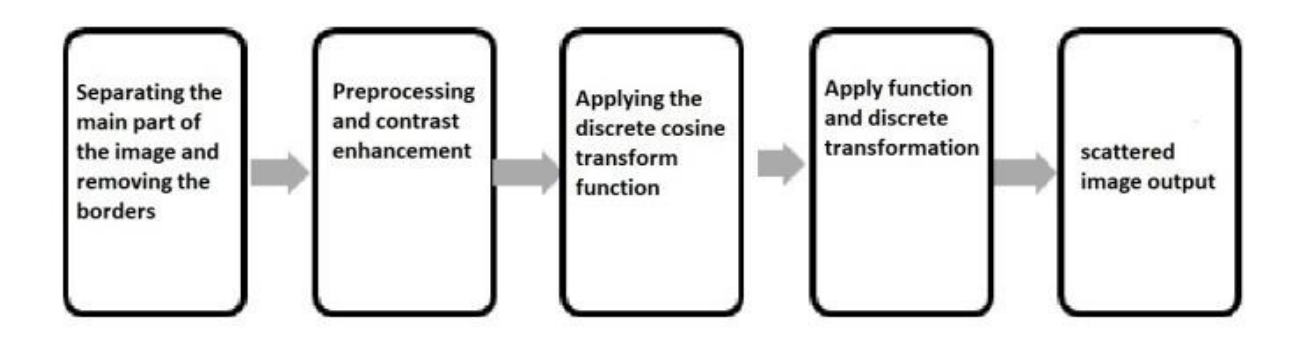


Fig. 7. The process of applying the discrete cosine transformation function.

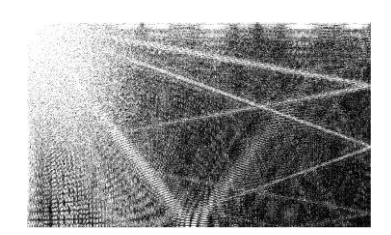


Fig. **8.** Image resulting from the DCT algorithm on the original image.

#### B.III. Features based on wavelet transform

Figure 9-a shows the wavelet transformation on the image and how to create the sub-image and related filters. Part B shows the division of the image. In this figure, the approximation of the image with A and sub-images, or in other words, the details of the image in high frequencies, H, are vertical details, D are diagonal details, and V are horizontal details in the image. If higher levels of wavelet transformation are needed, this transformation is applied in part a. The edges of the image are visible in the sub-bands obtained from this transformation in such a way that the horizontal, vertical, and diagonal edges are shown in each of the sub-images. If the fabric has damage, the edges in each corresponding sub-band will be shown more clearly. Figure 10 shows the scattered image created from the wavelet transform in different sub-bands.

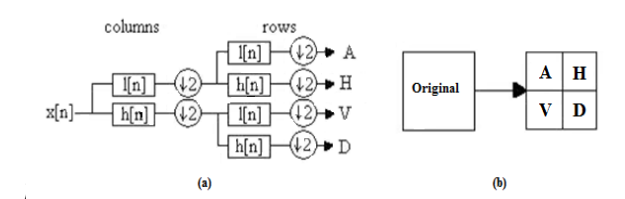


Fig. **9.** Block diagram of wavelet transformation on the image a) bank of filters, b) dividing the image into approximation and detail sub-bands.

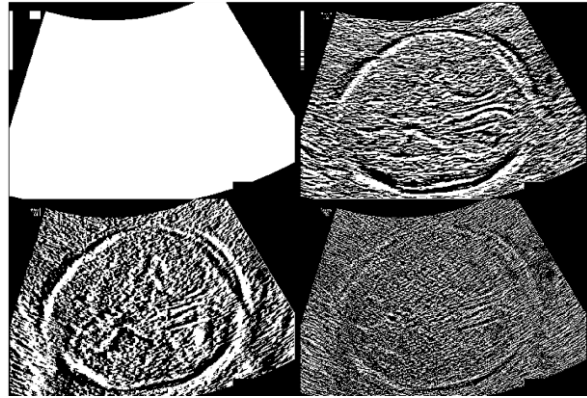


Fig. 10. Scattered image created by wavelet transform.

#### C. Feature integration

Three feature maps are created by applying the DCT algorithm, wavelet transform, and curve

scattering transform, and the selection of the best features plays an important role in the final segmentation. Merge rules are used to merge the image at the feature level. The most common rules used for image integration are the selection of maxima, minima, and finally, following averaging. The relationships represent these rules. In this thesis, the proposed method, as well as the other methods, each of which uses the integration law to select the maximum coefficients.

$$Selected_{def} = Max\{CURV_{def}(i.j).DCT_{def}(i.j).DWT_{def}(i.j)\}$$
(10)

 $Selected_{def}$  $= Min\{CURV_{def}(i.j).DCT_{def}(i.j).DWT_{def}(i.j)\}$  (11)

$$Selected_{def} = Avg\{CURV_{def}(i.j).DCT_{def}(i.j).DWT_{def}(i.j)\}$$
(12)

n the above equation,  $Selected_{def}$  is the output image after selecting the area in thefeature map.  $CURV_{def}(i.j)$  represents the feature map from resulting curve transformation.  $DCT_{def}(i,j)$  represents the map obtained from the DCT thinning transform and at the end,  $DWT_{def}(i,j)$  is discrete wavelet of transform feature map. Min: Max and Avg indicate the selection of minimum, maximum, and average. respectively. Max is used in this research.

#### D. Feature integration

Evaluation criteria play a decisive role in the feature selection. In other words, these criteria are the basis of feature selection. The selection of an optimal subset of the feature set directly depends on the appropriate selection of the evaluation criteria. In a way that, if any evaluation criterion assigns an inappropriate value to the subset of optimal features, this subset is never selected as the optimal subset. The values that different evaluation criteria give to a subset are different. In the concept of classification and its related issues, an optimal criterion must have a Bayesian error rate. E(S) is calculated from equation 13. Equation 14 is also used in discrete space [29].

$$E(s) = \int_{S} P(s)(1 - \max(P(c_i | S)))ds$$
or  $\sum_{S} (1 - \max(P(c_i | S)))$  (14)

$$or \sum_{S} (1 - \max(P(c_i \mid S)))$$
 (14)

As can be seen from equations 13 and 14, E(S)is desired as a sum or integral and is also nonlinear and non-negative. In equation 15, the upper bound of E(S) is calculated, H(C|S) the conditional entropy C in each S is given.

$$E(s) \le \frac{H(C \mid S)}{2} \tag{15}$$

Calculating E(S) directly is very difficult because S is a combination of features. As a result, most researchers prefer to use criteria based on correlation and distance. Equation 16, shows the evaluation criterion of the correlation coefficient. The covariance of the variables a and b is the variance.

$$r(a,b) = \frac{\text{cov}(a,b)}{\sqrt{\text{var}(a)}\sqrt{\text{var}(b)}}$$
(16)

Pearson's correlation coefficient is calculated in equation 17.

$$r(a,b) = \frac{N\sum a_i b_i - \sum a_i \sum b_i}{\sqrt{N\sum a_i^2 - \left(\sum a_i\right)^2} \sqrt{N\sum b_i^2 - \left(\sum b_i\right)^2}} (17)$$

Mutual Information (MI) is obtained from equation 18. p(0) is Probability Density Function (PDF).

$$I(a,b) = \sum_{a} \sum_{b} p(ab) \log \frac{p(ab)}{p(a)p(b)}$$
 (18)

Equation 19, illustrates symmetric uncertainty (SU). H (0) is the entropy of each feature.

$$SU(a,b) = \frac{2I(a;b)}{H(a) + H(b)}$$
 (19)

Distance information is calculated in equation 20. H(a|b) is the conditional entropy a in term b.

$$d(a,b) = \frac{H(a|b) + H(b|a)}{2}$$
 (20)

Finally, the last criterion, which is very common for evaluation, is calculated from equation 21, and it is the Euclidean distance criterion.

$$d(a,b) = \sqrt{\sum (a_i - b_i)^2}$$
 (21)

These common criteria are used to evaluate feature selection methods. Although there are other criteria, such as Laplacian score, Fisher Score [30], and other criteria, information criteria require features in a discrete state, and discretization is required if they are used [31].

#### E. Classification

For the experiment, three different machine learning algorithms were used together: support vector machine (SVM), K-nearest neighbors (KNN), ensemble method, and random forest (RF).

SVM is a statistically supervised learning algorithm. It was originally developed for regression work but later used for linear and non-linear classification. In an SVM, the cloud that defines the boundary in the data space is trained to maximize the distance to the nearest data. SVMs can have higher performance in classification and regression problems than other statistical and ML techniques.

KNN is a widely used method for data mining. This method determines the similarity between the new data and the existing data and groups the new data into groups similar to the existing data. The algorithm works on this basis.

- 1. Choosing the number of K neighbors.
- 2.Calculate the "Euclidean distance", which is to measure the distance between any two points. Formula like equation 22.

$$D = \sqrt{((X_2 - X_1)^2 + (Y_2 - Y_1)^2)}$$
 (22)

- 3. From the calculation in step 2.
- 4. The bundle for a new data point is assigned to the maximum number of neighbors.

RF random forest is a group algorithm that uses bagging as a set method and decision tree as an individual method, thus helping to reduce variance and bias in improved findings. The classifier combines multiple decision trees and a more robust classification with better generalization and easier hyperparameter tuning to overcome overfitting problems. For classification tasks in RF, each tree provides a classification or takes a "vote".

#### IV. EVALUATION

In this article, a new method based on image thinning features and common classifications is proposed. In the following, the proposed method will be evaluated with common evaluation criteria. The system used for simulation is an Intel processor system. The desired hardware is a 5-core (Core<sup>TM</sup>) i7 CPU with a working frequency of 2.60GHz. 8 GB of RAM. The Windows 10 operating system is installed on this system. The software used is MATLAB 2022b. To classify the integrated features, the mutual validation method is used with a factor of 10 (K=10), which means that the data is first divided into 10 equal categories (because the factor of 5 has a better bias and considering that the number the registrations were 120, the test coefficient was 30%, and the training was 70%. In each stage, one group out of 10 categories is used for testing and four other categories are used for training, and finally, the average is made between the 10 classification indicators of the test. This process is generally shown in Figure 11.

Fig. 11. Cross-validation method from the tenth rank.

The proposed method is analyzed using a variety of Accuracy and Precision evaluation criteria. These two criteria are among the most significant evaluation criteria for diagnosis and classification. Therefore, these two criteria are used in this research. Two accuracy and precision evaluation criteria, recall rate and sensitivity, and F-Measure are introduced and calculated according to equations 23 and 27 and used to evaluate the system [32].

$$Re \, call = \frac{TP}{TP + FN}$$

$$ACC = \frac{TN + TP}{TN + TP + FN + FP}$$
(23)

$$ACC = \frac{TN + TP}{TN + TP + FN + FP} \tag{24}$$

Specificity = 
$$\frac{TN}{TN + FP}$$
 (25)

$$F\_Measure = \frac{2 \times TP}{2 \times TP + FP + FN}$$
 (26)

In these equations, TP, is true positive, TN, is true negative, FP, is false positive, and FN, is false negative.

#### A. Databases

A dataset will be used in this paper. Fetal head ultrasound is a dataset for measuring fetal head circumference (HC), ultrasound imaging used to measure fetal biometrics during pregnancy. The dataset is part of the HC18 challenge and contains a total of 1334 two-dimensional (2D) ultrasound images of a standard plane that can

be used to measure HC. All two-dimensional (2D) ultrasound images of HC were collected from the database of the Department of Gynecology, Obstetrics and Radboud University Medical Center, Nijmegen, The Netherlands. Ultrasound images were obtained from 551 pregnant women who received a routine ultrasound screening examination between May 2014 and May 2015. Only embryos that did not show any developmental abnormalities were included in this study. **Images** were obtained by experienced sonographers using a Voluson E8 or Voluson 730 ultrasound machine (General Electric, Austria). CMO Arnhem-Nijmegen approved the collection and use of these data for this study. Due to retrospective data collection, informed consent was waived. All data were anonymized according to the principles of the Declaration of Helsinki. The size of each 2D ultrasound image was 800 x 540 pixels, with pixel sizes ranging from 0.052 to 0.326 mm. This large variation in pixel size is the result of ultrasound settings by the sonographer (depth and zoom settings typically vary during the exam) to account for different fetal sizes. The size of each 2D ultrasound image was 800 x 540 pixels, with pixel sizes ranging from 0.052 to 0.326 mm. This large variation in pixel size is the result of ultrasound adjustments by the sonographer (depth and zoom settings typically

vary during the exam) to account for different fetal sizes. Figure 12 shows sample ultrasound images from each trimester. The distribution of GA in this study is shown in Figure 12. Most of the data were obtained after 12 and 20 weeks of gestation, as these are the standard times for routine ultrasound screening for pregnant women in the Netherlands. During each sonographer examination, the manually annotated the HC. This was done by drawing an ellipse that best fit the head circumference. Figure 12 also shows a comparison between the HC distribution and the Verburg et al. growth curve. The reference GA was determined by measuring the CRL between 20 mm (8+4 weeks) and 68 mm (12+6 weeks). This database is available at https://datasetninja.com/fetalhead-ultrasound.

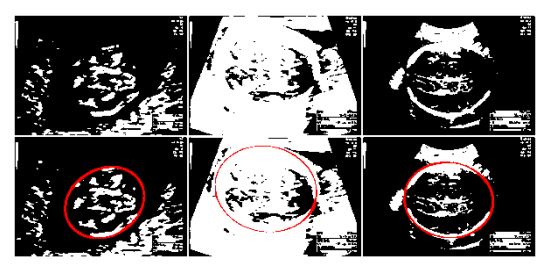


Fig. 12. Some images in the database.

#### B. Results

Table 1, shows the test accuracy and validity loss of the proposed network with three tests in multi-class AD classification. The average of each time in the detection of each state is also determined. It is important to repeat the experiment to show that the results obtained are not random. The best average test accuracy is obtained with the proposed network in the second run. Table 2 shows the final evaluation results in more detail and in each test in terms of accuracy, recall rate, F criterion, and AUC criterion.

Table 1.Comparison of the accuracy of fetal brain health diagnosis in different implementations with different classifications.

Class Name	SVM	KNN	RF
Normal	0.9593	0.9688	0.9900
Suspicious	0.9984	0.9999	0.9685
Sick	0.9729	0.9801	0.9801

Figure 13 shows the comparison of accuracy in different conditions of fetal brain health in three tests, as well as the average value. As can be seen in Figure 13, the accuracy of diagnosis in all stages is more than 98%. This is important because of the entry of the most informative bands of the image into the proposed deep neural network, and also the settings made in the proposed deep network.

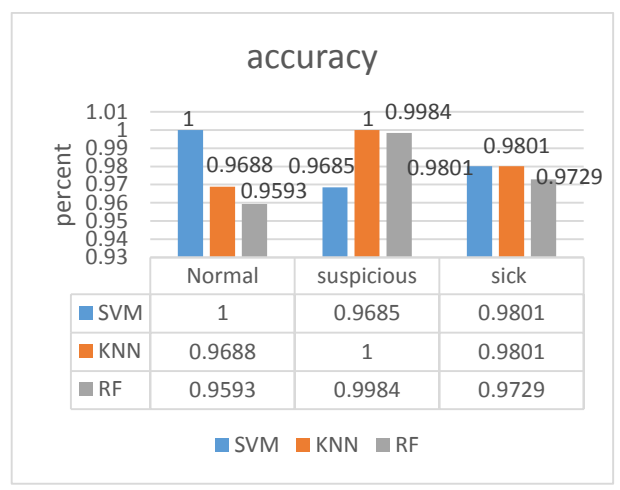


Fig. 13. Graphical comparison of the results in detection accuracy.

Table 2. Comparison of the results obtained in different tests in the rest of the criteria

tests in the rest of the criteria.				
Evaluation	Clas			
Criteria	S	Normal	Suspicious	Sick
Criteria	Name			
	SV	0.9979	0.9984	1.0000
	M			
Precisio	KN	0.9988	0.9999	1.000
n	N			0
	RF	0.8964	1.0000	1.0000
	SV	0.9593	0.9729	0.9713
	M			
D 11	KN	0.9686	0.9801	0.9781
Recall	N			
	RF	1.0000	0.9801	0.9740
	SV	0.9782	0.9855	0.9854
	M			
F-	KN	0.9836	0.9899	0.9899
Measure	N			
	RF	0.9454	0.9899	0.9868
	SV	0.9994	0.9995	0.9996
	M			
ATIO	KN	0.9996	0.9997	0.9997
AUC	N			
	RF	0.9996	0.9997	0.9997

Figure 14, shows the comparison of accuracy, figure 15, compares the recall rate, figure 16, compares the F criterion and figure 17, shows the comparison of AUC in different states of fetal brain health in three tests with three categories used.

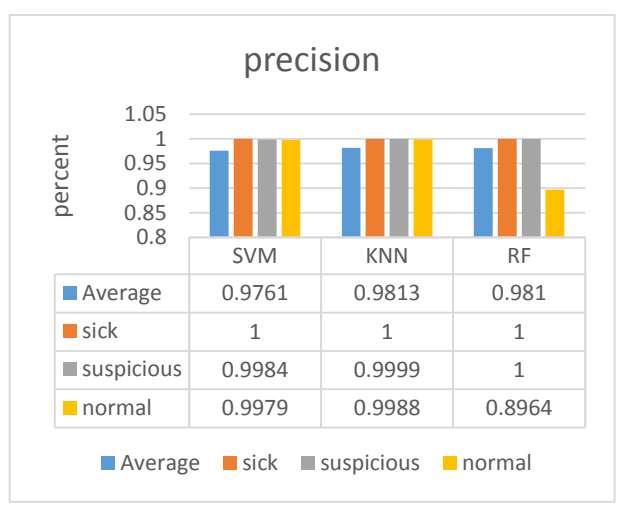


Fig. **14.** Comparison of the accuracy of fetal brain health diagnosis for each category

As seen in these figures, the criteria obtained in all stages are more than 98%. This is important because of the inclusion of the most informative features in the desired and proposed classifications, as well as the adjustments made in the proposed method.

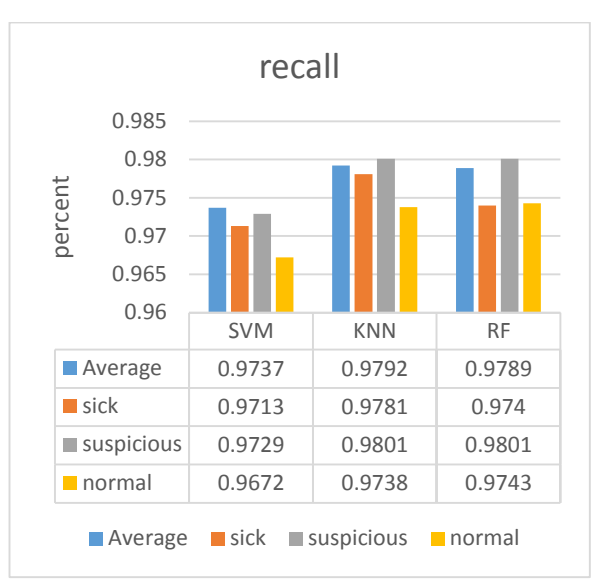


Fig. **15.** Comparison of the recall rate of fetal brain health diagnosis for each category.

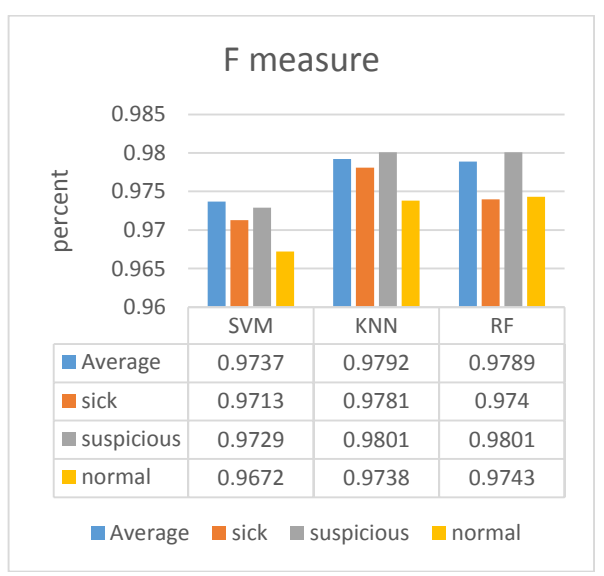


Fig. **16.** Comparison of the F criteria for diagnosing fetal brain health status for each category.

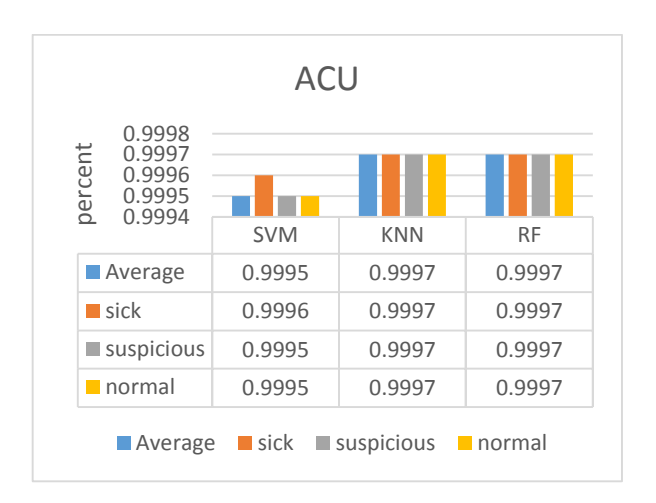


Fig. 17. Comparison of the AUC criterion for detecting fetal brain health status in each test.

#### C. Comparison with other research

The proposed performance was evaluated three times with three different categories. Also, the results obtained were compared with [33]. This research has been divided into two groups: healthy and sick. To make a comparison, using the same data sample, data partitioning, and the number of steps, an additional evaluation is compared with the Alex Net training used on the dataset [34]. The classification results have been evaluated in terms of the average classification precision and accuracy of each AD stage. Table 3 provides a comparative analysis and also summarizes the classification results with other approaches.

Table 3. Comparison with the reference [35]in diagnosing fetal brain health status.

Pathology	[35]	SVM	KNN	AlexNet
Normal	98.34	100.0	96.88	91.73
Suspicious	94.55	96.85	100.0	100.0
Sick	94.97	98.01	98.01	95.14

In the comparative analysis, the proposed model has performed better than [34]and the trained AlexNet model. In all implementations, the accuracy and correctness of the proposed method are much better. The reason for this is the use of the most informative scattered extracted features with the help of the selection of the proposed feature and the settings made on the proposed method. In order to further evaluation, the proposed method has been compared with the other methods of diagnosing fetal brain health status, which have been done by other researchers. The database of these studies is the same in Table 4. In [36], deep learning based on support vector machines [37], deep learning based on convolutional neural networks [38] are compared. The results obtained in accuracy in the three cases compared show the superiority of the proposed method in diagnosing the progress of the disease stage.

#### V. CONCLUSION

Early diagnosis of fetal diseases is very important to improve the quality of life of people after birth and to develop improved treatment and targeted drugs.

Table 4. Comparison with other research in different situations.

Reference	Subjects	Task	ACC
[36]	43,890 images, 16,463 subjects	Sick again NL	94.10 87.14 85.85
[37]	INTERGROWTH21st dataset INTERBIO-21st dataset [40]	Sick again NL	97.79 94.73 42.70
[38]	INTERGROWTH21st dataset INTERBIO-21st dataset [40]	Sick again NL	96.47 88.47 80.17
Proposed D2 Model	INTERGROWTH21st dataset INTERBIO-21st dataset [40]	Sick again NL	98.61 98.67 98.87

In this article, the purpose of investigating the effectiveness of ultrasound imaging advanced machine learning techniques for the classification and diagnosis of multiple classes of fetal health was carried out. This study proposed the use of various machine learning classifiers along with various features based on the thinning transformation to perform 3-class classification. The proposed method was trained three times separately on single-channel ultrasound images. Using the proposed method helped to achieve better performance. The results of this study show that the integration of imaging methods and machine learning can help to make diagnostic decisions in the early diagnosis of fetal diseases. Diagnosing fetal health status can aid drug discovery by providing better pathogenesis to measure the effects of targeted therapies that can slow disease progression. By combining clinical imaging with machine learning techniques, we can help uncover patterns of functional changes in the brain associated with the development of fetal health and can help identify risk factors and prognostic indicators.

#### REFERENCES

- [1] Z. Alfirevic, G. M. Gyte, A. Cuthbert, and D. Devane, "Continuous cardiotocography (CTG) as a form of electronic fetal monitoring (EFM) for fetal assessment during labour," *Cochrane database of systematic reviews*, no. 2, 2017.
- [2] N. Muhammad Hussain ,A. U. Rehman, M. T. B. Othman, J. Zafar, H. Zafar, and H. Hamam, "Accessing artificial intelligence for fetus health status using hybrid deep learning algorithm (AlexNet-SVM) on cardiotocographic data," *Sensors*, vol. 22, no. 14, pp. 5103, 2022.
- [3] K. Barnova, R. Martinek, R. Vilimkova Kahankova, R. Jaros, V. Snasel, and S. Mirjalili, "Artificial Intelligence and Machine Learning in Electronic Fetal Monitoring," *Archives of Computational Methods in Engineering*, pp. 1-32, 2024.
- [4] M. Vafaeezadeh, H. Behnam, and P. Gifani, "Ultrasound Image Analysis with Vision Transformers–Review," 2024.
- [5] M. C. Fiorentino, F. P. Villani, M. Di Cosmo, E. Frontoni, and S. Moccia, "A review on deep-learning algorithms for fetal ultrasound-image analysis," *Medical image analysis*, vol. 83, pp. 102629, 2023.
- [6] P. H. Diniz, Y. Yin, and S. Collins, "Deep learning strategies for ultrasound in pregnancy," *European Medical Journal*. *Reproductive health*, vol. 6, no. 1, pp. 73, 2020.
- [7] P.-H. Yeung, L. S. Hesse, M. Aliasi, M. C. Haak, W. Xie, A. I. Namburete, and I.-s. "Sensorless Consortium, volumetric reconstruction of fetal brain freehand scans with deep ultrasound implicit representation," Medical Image Analysis, vol. 94, pp. 103147, 2024.
- [8] S. MolinaGiraldo, N. TorresValencia, C. TorresValencia, and H. F. Restrepo, "Anatomical structure characterization of fetal ultrasound images using texture based segmentation technique via an interactive MATLAB application," *Journal of Clinical Ultrasound*, vol. 52, no. 2, pp. 189-20. Y Y Y Y
- [9] H. P. Kim, S. M. Lee, J.-Y. Kwon, Y. Park, K. C. Kim, and J. K. Seo, "Automatic evaluation of fetal head biometry from ultrasound images using machine learning," *Physiological measurement*, vol. 40, no. 6, pp. 065009, 2019.

- [10] J. Yu, Y. Wang ,P. Chen, and Y. Shen, "Fetal abdominal contour extraction and measurement in ultrasound images," *Ultrasound in medicine & biology*, vol. 34, no. 2, pp. 169-182, 2008.
- [11] Z. Cömert, A. F. Kocamaz, and V. Subha, "Prognostic model based on image-based time-frequency features and genetic algorithm for fetal hypoxia assessment," *Computers in biology and medicine*, vol. 99, pp. 85-97, 2018.
- [12] S. Thomas, and S. Harikumar, "An ensemble deep learning framework for foetal plane identification," *International Journal of Information Technology*, pp. 1-10, 2024.
- [13] M. Alzubaidi, U. Shah, M. Agus, and M. Househ, "FetSAM: Advanced Segmentation Techniques for Fetal Head Biometrics in Ultrasound Imagery," *IEEE Open Journal of Engineering in Medicine and Biology*, 202.5
- [14] M. Lin, Q. Zhou, T. Lei, N. Shang, Q. Zheng, X. He, N. Wang, and H. Xie, "Deep learning system improved detection efficacy of fetal intracranial malformations in a randomized controlled trial," *NPJ Digital Medicine*, vol. 6, no. 1, pp. 191, 2023.
- [15] V. Nagabotu, and A. Namburu, "Precise segmentation of fetal head in ultrasound images using improved U- Net model," *ETRI Journal*, 2023.
- [16] H. Ghabri, M. S. Alqahtani, S. Ben Othman, A. Al-Rasheed, M. Abbas, H. A. Almubarak, H. Sakli, and M. N. Abdelkarim, "Transfer learning for accurate fetal organ classification from ultrasound images: a potential tool for maternal healthcare providers," *Scientific Reports*, vol. 13, no. 1, pp. 17904, 2023.
- [17] M. C. Walker, I. Willner, O. X. Miguel, M. S. Murphy, D. El-Chaâr, F. Moretti, A. L. Dingwall Harvey, R. Rennicks White, K. A. Muldoon, and A. M. Carrington, "Using deeplearning in fetal ultrasound analysis for diagnosis of cystic hygroma in the first trimester," *Plos one*, vol. 17, no. 6, pp. e0269323, 2022.
- [18] Y. Zhou, "Prediction and value of ultrasound image in diagnosis of fetal central nervous system malformation under deep learning algorithm," *Scientific Programming*, vol. 2021, pp. 1-7, 2021.
- [19] P. Deepika, R. Suresh, and P. Pabitha, "Defending Against Child Death: Deep learning based diagnosis method for abnormal

- identification of fetus ultrasound Images," *Computational Intelligence*, vol. 37, no. 1, pp. 128-154, 2021.
- [20] X. P. Burgos-Artizzu, D. Coronado-Gutiérrez, B. Valenzuela-Alcaraz, E. Bonet-Carne, E. Eixarch, F. Crispi, and E. Gratacós, "Evaluation of deep convolutional neural networks for automatic classification of common maternal fetal ultrasound planes," *Scientific Reports*, vol. 10, no. 1, pp. 10200, 2020.
- [21] R. Qu, G. Xu, C. Ding, W. Jia, and M. Sun, "Deep learning-based methodology for recognition of fetal brain standard scan planes in 2D ultrasound images," *Ieee Access*, vol. 8, pp. 44443-44451, 2019.
- [22] P. Durka, M. Dovgialo, A. Duszyk-Bogorodzka, and P. Biegański, "Two-Stage Atomic Decomposition of Multichannel EEG and the Previously Undetectable Sleep Spindles," *Sensors*, vol. 24, no. 3, pp. 842, 2024.
- [23] B. A. Olshausen, and D. J. Field, "Sparse coding with an overcomplete basis set: A strategy employed by V1?," *Vision research*, vol. 37, no. 23, pp. 3311-3325, 1997.
- [24] M. Aharon, M. Elad, and A. Bruckstein, "K-SVD: An algorithm for designing overcomplete dictionaries for sparse representation," *IEEE Transactions on signal processing*, vol. 54, no. 11, pp. 4311-4322, 2006.
- [25] J. Stromberg, "A Modified Haar System and Higher Order Spline Systems; Conf. in Honor of A. Zygmund," *Wadsworth Math. Series*, pp. 475-493, 1981.
- [26] Y. Meyer, "Principe d'incertitude, bases hilbertiennes et algebres d'operateurs," *Séminaire Bourbaki*, vol. 662, 1986.
- [27] I. Daubechies, "Orthonormal bases of compactly supported wavelets," *Communications on pure and applied mathematics*, vol. 41, no. 7, pp. 909-996, 1988.
- [28] G. Beylkin, "On the representation of operators in bases of compactly supported wavelets," *SIAM Journal on Numerical Analysis*, vol. 29, no. 6, pp. 1716-1740, 1992.
- [29] A. Benkessirat, and N. Benblidia, "Fundamentals of feature selection: An overview and comparison." pp. 1-6.

- [30] M. A. Valizade Hasanloei, R. Sheikhpour, M. A. Sarram, E. Sheikhpour, and H. Sharifi, "A combined Fisher and Laplacian score for feature selection in QSAR based drug design using compounds with known and unknown activities," *Journal of Computer-Aided Molecular Design*, vol. 32, no. 2, pp. 375-384, 2018.
- [31] M. Azhar, and P. A. Thomas, "Comparative review of feature selection and classification modeling." pp. 1-9.
- [32] S. Qi, X. Wu, W.-H. Chen, J. Liu, J. Zhang, and J. Wang, "sEMG-based recognition of composite motion with convolutional neural network," *Sensors and Actuators A: Physical*, vol. 311, pp. 112046, 2020.
- [33] V. Gude, and S. Corns, "Integrated deep learning and supervised machine learning model for predictive fetal monitoring," *Diagnostics*, vol. 12, no. 11, pp. 2843, 2022.
- [34] R. Sreelakshmy ,A. Titus, N. Sasirekha, E. Logashanmugam, R. B. Begam, G. Ramkumar, and R. Raju, "[Retracted] An Automated Deep Learning Model for the Cerebellum Segmentation from Fetal Brain Images," *BioMed Research International*, vol. 2022, no. 1, pp. 8342767, 2022.
- [35] Y. Kazemi, and S. Houghten, "A deep learning pipeline to classify different stages of Alzheimer's disease from fMRI data." pp. 1-8.
- [36] H. Xie, N. Wang, M. He, L. Zhang, H. Cai, J. Xian, M. Lin, J. Zheng, and Y. Yang, "Using deep-learning algorithms to classify fetal brain ultrasound images as normal or abnormal," *Ultrasound in Obstetrics & Gynecology*, vol. 56, no. 4, pp. 579-587, 2020.
- [37] M. Lin, X. He, H. Guo, M. He, L. Zhang, J. Xian, T. Lei, Q. Xu, J. Zheng, and J. Feng, "Use of real- time artificial intelligence in detection of abnormal image patterns in standard sonographic reference planes in screening for fetal intracranial malformations," *Ultrasound in Obstetrics & Gynecology*, vol. 59, no. 3, pp. 304-316, 2022.
- [38] L. H. Lee, E. Bradburn, R. Craik, M. Yaqub, S. A. Norris, L. C. Ismail, E. O. Ohuma, F. C. Barros, A. Lambert, and M. Carvalho, "Machine learning for accurate estimation of fetal gestational age based on ultrasound images," *NPJ digital medicine*, vol. 6, no. 1, pp. 36, 2023.

- [39] W. Li, X. Lin, and X. Chen, "Detecting Alzheimer's disease Based on 4D fMRI: An exploration under deep learning framework," *Neurocomputing*, vol. 388, pp. 280-287, 2020.
- [40] J. Villar, R. B. Gunier, C. O. Tshivuila-Matala, S. A. Rauch, F. Nosten, R. Ochieng, M. C.

Restrepo-Méndez, R. McGready, F. C. Barros, and M. Fernandes, "Fetal cranial growth trajectories are associated with growth and neurodevelopment at 2 years of age: INTERBIO-21st Fetal Study," *Nature Medicine*, vol. 27, no. 4, pp. 647-652, 2021.

THIS PAGE IS INTENTIONALLY LEFT BLANK.